Research Square

Preprints are preliminary reports that have not undergone peer review.
They should not be considered conclusive, used to inform clinical practice,
or referenced by the media as validated information.

CASINO Predictions of Polyethylenimine Nanofiber Sample Preparations for SEM

Brandi J. Cook

b.jcook@usf.edu

University of South Florida

Wayne C. Guida

University of South Florida

Sylvia W. Thomas

University of South Florida

Research Article

Keywords: Nanofiber, SEM, CASINO, electron trajectory, SEM sample preparation, Polyethylenimine, Electrospinning, Scanning electron microscopy (SEM), CASINO (Monte CArlo SImulations of electroN trajectory in sOlid), Energy Dispersive X-ray Spectrometer (EDS/EDX), AI

Posted Date: November 18th, 2026

DOI: https://doi.org/10.21203/rs.3.rs-11555141/v1

License: This work is licensed under a Creative Commons Attribution 4.0 International License.
Read Full License

Additional Declarations: No competing interests reported.

CASINO Predictions of Polyethylenimine Nanofiber Sample Preparations for SEM

Brandi J. Cook, MS [1], **Wayne C. Guida, PhD** [2] and **Sylvia W. Thomas, PhD** [3]

[1] Department of Chemistry, and Cell Biology, Microbiology, and Molecular Biology, in the College of Arts and Sciences, University of South Florida, Tampa, FL, USA; ORCID #: 0000-0003-2681-7409

[2] Department of Chemistry, College of Arts and Sciences, University of South Florida, Tampa, FL, USA

[3] Department of Electrical Engineering, College of Engineering, and Research and Innovation, University of South Florida, Tampa, FL, USA

Primary/ Corresponding Author E-mail: [1] bjcook@usf.edu;

Contributing Author(s) E-mail(s): [2] wguida@usf.edu; [3] sylvia@usf.edu

Abstract

This study presents a method of predetermining the necessary sample preparations, and parameter settings to set a Scanning Electron Microscope (SEM) for optimal visual detection of morphological imaging of micro- and nanostructured biodegradable polymers, such as polyethylenimine (PEI) nanofiber, cross-section diameters between 50-500nm. Computational predictions of simulated SEM micro and nano scale images can provide optimization for the characterization of material systems and provide a complementary research observation for training artificial intelligence (AI) models, reducing trial-and-error experimental testing. Micro and nano scale fibers with cross-sectional diameters between 50-500nm serve as building blocks for membrane materials for medical, energy, space, and military applications. This method utilizes the computational prediction software, Monte **CA**rlo **SI**mulations of electro**N** trajectory in s**O**lid (**CASINO**), to predetermine mounting base and sample coating material for the sample as well as the of number of electrons and voltage of the electron beam from the SEM. The method of employing CASINO reduces the optimization needed to lessen trapped incident beam electrons, electron overcharging of the sample and deterioration of samples during SEM use and provide insight into improving SEM images of various layered materials. Sample preparation optimization using CASINO agrees with consistently used parameters and narrows the range for incongruency across studies, supporting a fabrication standard for increased yield verse expended product used for SEM verification purposes.

Keywords: Nanofiber, SEM, CASINO, electron trajectory, SEM sample preparation, Polyethylenimine, Electrospinning, Scanning electron microscopy (SEM), CASINO (Monte CArlo SImulations of electroN trajectory in sOlid), Energy Dispersive X-ray Spectrometer (EDS/EDX), AI

List of Abbreviations

AE ..... Absorbed Electrons

Ag ..... Silver

AI ..... Artificial Intelligence

Al ..... Aluminum

AMBIR ..... Advanced Materials Bio and Integration Research

Au ..... Gold

B ..... Apparent Brightness

B-PEI ..... Branched Polyethylenimine

BSE ..... Backscattered Electrons

C ..... Carbon

CASINO ..... Monte **CA**rlo **SI**mulations of electro**N** trajectory in s**O**lid

CMMB ..... Cellular Biology, Microbiology and Molecular biology

dTE ..... detectable TE

EBSD ..... Electron Backscatter Diffraction

EDS/EDX ..... Energy Dispersive X-ray Spectrometer

Bc ..... Emission Brightness

H ..... Hydrogen

N ..... Nitrogen

NREC ..... Nanotechnology Research and Education Center

NF ..... Nanofiber

NSF ..... National Science Foundation

O ..... Oxygen

PEI ..... Polyethylenimine

PEI NF ..... Polyethylenimine Nanofiber

PEO ..... Polyethylene Oxide

PI ..... Professor Investigator

PLGA ..... Poly Lactic-co-Glycolic Acid

PVA ..... Poly (Vinyl Alcohol)

RET ..... Research Experience for Teachers

REU ..... Research Experience for Undergraduates

SE ..... Secondary Electrons

SEM ..... Scanning Electron Microscope

TE ..... Transmitted Electrons

Va ..... Accelerating Voltage

Ve ..... Amount of Electrons of the Initial Beam

USF ..... University of South Florida

V ..... Version

V2 ..... Version 2

V3 ..... Version 3

Z ..... Atomic Number

2D ..... 2 Dimensional

3D ..... 3 Dimensional

Symbols

* ..... asterisk symbol representing TE (dTE)

^ ..... caret symbol representing AE

‡ ..... diesis symbol representing SE

η ..... emission coefficient

† ..... obelisk symbol representing BSE

Units

cm^3 .....centimeters cubed

eV .....electrovolts

g .....grams

keV .....kiloelectronvolt

kV .....kilovolt

μm ..... micrometer

nm ..... nanometers

Pa .....pascal

Table of Contents

Title 1

Abstract & Key Words 2

List of Abbreviations 3

Table of Contents 6

1. Introduction 7

2. Methods 15

2.1 Electron Trajectory Output Defined 19

3. Results 20

3.1 Electron Trajectories upon a single PEI NF 21

3.2 Electron Trajectories of Differing keV upon Modeled Sample Types of Increased NF sample Number & Aluminum backed Sample 24

3.3 Comparison of Electron Trajectories of Differing keV upon Gold coated & Aluminum backed Model Sample 27

4. Discussion 35

4.1 Comparison of Published Works 35

5. Conclusion and Future Directions 38

5.1 Other methods to obtaining better resolution SEM at low voltage for organic samples 42

6. Supplementary Material 45

7. Declarations 47

7.1 Data Availability 47

7.2 Authors Affiliations (COI) 47

7.3 Author Contributions & Acknowledgements.....51

7.4 Funding & Competing Interests.....51

7.5 Clinical Trial & Ethics Statement.....52

8. References.....52

1. Introduction

Scanning Electron Microscopy (SEM) uses electron path detection, of electrons that collide, penetrate, spread and escape the incidence of sample contact, to be detected in a scanning manner for the production of a visual representation of the sample [1, 2]. SEM generates electrons from the source of the electron beam to the sample. The backscattered electrons (BSE) and secondary electrons (SE) generated are received by the detectors, which give the samples atomic number/phase contrast and topographical signals respectively, for the computer visualization results that are received from the electron paths produced with the parameters chosen [2-5].

The information detected by SEM from the sample varies significantly depending upon the samples chemical composition and parameters chosen. The parameters for number of electrons, and voltage of the electron beam are different for each sample/elemental composition type. Some sample types that are biological, powder, or non-conductive, require prior preparation to become conductive and produce the types of electron pathways that are detectable by the SEM. Non-conductive samples, such as a biological one, can trap the incident beam electrons on the surface

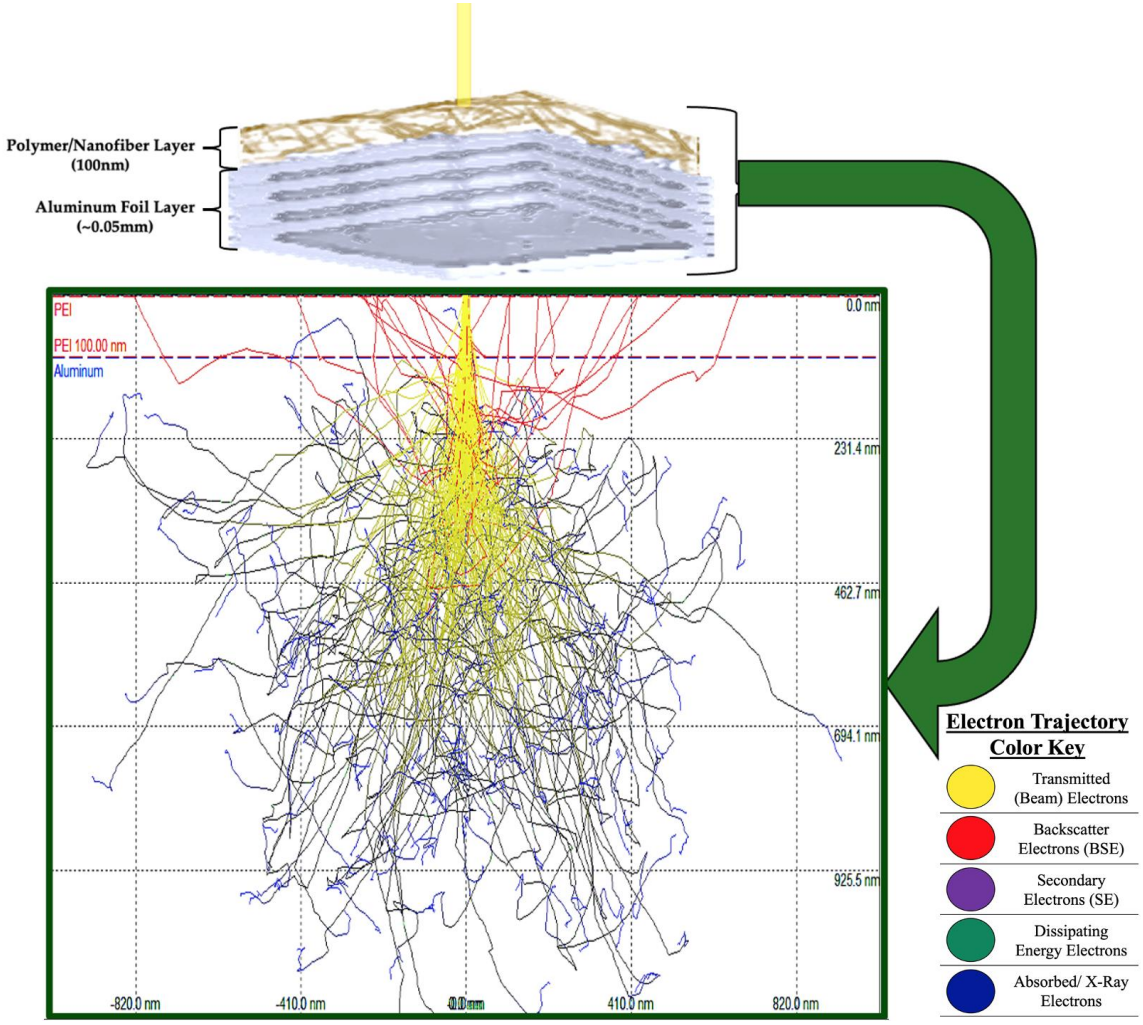
and result in a built-up of charge that can cause overt brightness that overpowers imaging (overheating), as well as sample deterioration of up to 10nm [2-4, 6, 7].

A biodegradable polymer sample, that is between 50-500nm, can easily degrade under the bombardment of electrons in the SEM in a short period of time, which causes limits to capturing clear image scans. In order to save the loss of yield of the sample, prior to SEM electron-sample interactions, preparing the sample for electron incidence is necessary [2, 7]. This can be done by simulating the beneficial sample preparations and SEM settings to make prior, for optimal SEM imaging. To predict what parameters are necessary for the clearest visible detection of a biodegradable nanofiber (NF) a SEM computational prediction software, Monte **CA**rlo **SI**mulations of electro**N** trajectory in s**O**lid (**CASINO**), was employed [8-13].

CASINO software is a reliable SEM electron trajectory predictor due to its use of Monte Carlo calculations, in which a randomized numerical selection is made to produce variance in a repeated test under the same conditions that creates a scattered selection (under a Gaussian curve predicated distribution) of the probable results, such as electron trajectories, emitting under the same conditions to the same sample but traveling along a different path of trajectory [7, 8, 14-16]. The original CASINO code for the following described results were obtained through 'R. J. Needs, M. D. Towler, N. D. Drummond and P. R. C. Kent, CASINO version 1.7 User Manual, University of Cambridge, Cambridge (2004)' [8]. CASINO version 2 (V2) had 2D (2 dimensional) sample capability and CASINO version 3 (V3) has 3D (3 dimensional) sample modeling capability [9, 11-13, 17]. The diameter of a NF is approximately 100nm, and when modeled within the 2D space it is difficult to visualize the electron incidence of contact. As seen

in **Figure 1. CASINO version 2 (2D) simulation**, in which the electron beam, of 100 electron trajectories, at 20keV (kiloelectronvolt) is simulated to penetrate a 100nm PEI solid sample atop a ~0.05nm Aluminum (Al) surface.

Figure 1. CASINO version 2 (2D) simulation



[Figure 1 CASINO version 2 (2D) simulation] Electron beam, of 100 electrons, at the velocity of 20keV is simulated to penetrate a 100nm PEI sample (indicated by red text on the top left of V2 2D output) atop a ~0.05nm aluminum (Al) surface (indicated by blue text on the top left of V2 2D output). V2 2D output x-axis indicates the horizontal distribution in nm and y-axis indicates the vertical depth in nm of the electron beam [8, 11-13]. Electron trajectory keV are

color designated electron beams; initial transmitted beam electron trajectories (yellow), backscatter electrons (BSE; red), secondary electrons (SE; purple), dissipating energy electrons (green) and X-Ray electron incidences (blue; indicate absorbed electrons), from increasing to decreasing keV [2, 18].

Within the results of the 2D simulation, it is challenging to determine which electron trajectories initiate path changes for the NF layer incidence or for an Al base-layer incidence. To look further into this, the CASINO V3 was utilized to enhance the sample simulation, by first modeling a NF cylinder shape of an organic erodible single polyethylenimine nanofiber (PEI NF) sample, followed by the simulated beam effects [9].

This project demonstrates the software CASINO V3 3D being used to predict the reaction of 100 electron bombardments upon a biodegradable polymer sample, under varying conditions. The utilization of CASINO V3 models a cylindrical nanometer size organic erodible polyethylenimine (PEI) polymer sample, for predicting suitable SEM parameters [9]. The variables regarding the sample preparation are number of samples modeled, mounting base/stage material, and sample coating. The variable regarding SEM parameters, that is altered, is the velocity of the electron beam. Multiple simulations produced the results for comparison to the initial simulation run. The results allow for the investigation of the effects of changing one or more of the parameters that effect electron scattering (BSE and SE), as well as the signal generation within and escaping the sample [19, 20]. Information for absorbed electrons (AE) and transmitted electrons (TE), can also be obtained through the CASINO simulations as the electrons that have either been caught within the sample or have passed (directly or indirectly)

completely through the sample, respectively. This study entails why some parameters may not be as suitable for the sample types and how to test for a more SEM suitable preparation of the PEI NF sample, within the CASINO V3 software, prior to SEM analysis.

The sample of interest is a PEI NF. PEI is a single unit structure, that can form a linear or a branched polymer. The chemical contents of the repeating polymer units of PEI are an amine group (>NH), with two carbon ($-CH_2-CH_2-$) aliphatic spacers, with the density of 1.03g/cm^3. PEI interaction among itself is inevitable because of the charged cationic character of amines [21]. Commonly PEI is a co-polymer in bioerodible materials for structural support.

PEI is known for antimicrobial and antibiofilm activity, as one of its uses, and is in nanodrugs, in the forms of nanoparticles and NFs. Branched PEI (B-PEI) as a NF mat has shown antimicrobial and antibiofilm activity, with evidence of effects against bioactivities of antibiotic-resistant strains *Enterococcus faecium* and *Staphylococcus aureus* [22, 23]. Examples of PEI's other uses, are; in thermoresponsive cellulose and for CO_2 capture, in a project addressing climate change [24, 25]; PVA/B-PEI wound mats, addressed therapy against opportunistic pathogens (such as ESKAPE pathogens (*Enterococcus faecium, Staphylococcus aureus, Klebsiella pneumoniae, Acinetobacter baumannii, Pseudomonas aeruginosa, and Enterobacter spp*.) [22, 26, 27]); and PEO/PEI and PLGA with cisplatin and an antibody, in a multiaxial nanomembrane drug delivery system project addressing cancer therapy [28, 29]. PEI is also included in designs of materials to provide the desired properties such as weight, charge, and viscosity of a product. PEI is difficult to produce as a nanofiber without being combined with other small molecules and/or other polymers, or this maybe the perception due to not being able to observe the PEI NF at a nano scale in microscopic

machinery, due to the overlooked needs of properly preparing the NF sample with the appropriate backing, coating, and using a specific range of keV in the SEM, to visualize the PEI NF sample. The CASINO 3V capabilities address the prediction needs for a sample going into the SEM environment, for the better understanding of PEI properties independently as a NF, and the SEM image producing requirements for a NF PEI sample.

Within the SEM when an electron beam is triggered the electrons are accelerated in the direction of the beam along their path towards the sample staging area, within CASINO software the electron pathways are predicted. For the SEM image creation, the beam is set to dwell in a timed series, at a specific location on the sample, with each detection made at an area producing an image pixel made from the signals received, this continues in a scanning manner. The electron beam path is modified after emission by the SEM through apertures, lenses, and coils with magnetic and/or electrostatic forces to ensure beam diameter and direction for forming the successive scanned pattern. Due to the PEI NF samples size (50 -500nm diameter), a small beam diameter should be selected for greater special resolution of an image. The electrons (of short wavelengths and high energies) spread, hit the sample elastically scattering, and producing heat/charge where the beam meets the sample, this can destroy a biological sample (if the high vacuum chamber hasn’t). Excess signal of a high electron beam, exceeding the range of the SEM detectors through a high keV causes the relayed image to be overt brightness, indicative of sample charging. For non-biological samples high beam current (keV) increases the contrast quality but in the case of a PEI NFs it causes charging. Charging describes the build-up of the negative electron charge accumulating upon a surface of a non-conductive sample, such as a biological sample. This can negate the accurate detection of a sample by distorting the image, as

well as disqualify a sample control, between samples or within the same sample at differing sample locations. To prevent the degradation of an erodible sample by charging, an insensitive surface layer such as a metallic coating is needed to dissipate charging. The mounting base surface for the sample should also be metallic for the same reasons [7].

As the initial electron beam interacts with the sample surface some electron paths do not have a change of energy when passing through the sample. Those are **transmitted electrons** (**TE**) that are sourced from the beam not interacting with samples atoms, they exit from the sample or surroundings with their energy intact. CASINO 3V provides a subset of TE that is the predicted SEM captured particles as **detectable TE** (**dTE**). Electrons emitted from the electron beam that interact with the sample surface, become trapped and produce a charge are **absorbed electrons** (**AE**). AE create a current, a sample's electrons are excited from the ground state to higher energy states causing molecular changes. Too much of either TE and/or AE in SEM detection cause distorted image results. **Secondary electrons** (**SEs**) are electrons that have collided with an electron, hit and replacing an electron from an atom from the sample, scattering and deflecting electrons in an alternative direction. A fraction of SE energy decelerates after exiting the sample and it continues a path with lower kinetic energy. **Backscattered electrons** (**BSEs**) are electrons that have rebounded elastically from atomic interactions within the sample and the electrons kinetic energy is preserved. The subsequent electron paths are detected by electron detectors that are specialized in detecting BSEs vs. SEs electron paths. At some initial electron voltages, the incidence with the sample can produce X-Rays that are measured by energy dispersive X-ray spectrometer (EDS), which produces an X-ray spectrum of the sample for the

identification of the elemental contents of the specific sample. X-rays are produced when electrons hit the sample surface [7].

The goal is to obtain both BSEs and SEs, with as much yield as possible, as they are registered within the detectors for computation to produce the best scanned images of the compositional and topographic structures of the sample, in one setting. Biological materials are primarily composed of low atomic number (Z) elements (carbon, oxygen, nitrogen, hydrogen), which inherently provide low contrast in electron microscopy. To overcome this, biological samples are typically treated with compounds containing high Z elements, acting as stains [30]. BSEs discriminate between areas of high and low Z, their emission coefficient (η) monotonically increases with the Z of the sample material. This property establishes the physical basis for "Z-contrast" (or "compositional contrast") [3-5, 7]. Due to the direct relationship with Z, in biological samples treated with heavy metal stains or coating, BSEs can effectively highlight the stained regions, providing valuable compositional information and revealing ultrastructural details [7, 30] BSE signals are excellent for discriminating between areas of high and low Z and are particularly useful for imaging thin sections of biological samples, as they reveal areas treated with high Z stains or coating [7, 30]. SEs are the electrons that had inelastic collisions with atoms in the sample, ejecting weakly bound valence or conduction band electrons, which are useful for imaging that reveal surface topography and fine-scale details [2-5, 10]. SEs escape with lower energy and escape from shallow surface layers of the specimen, a few nanometers deep (2-5nm for metals, potentially deeper than 10nm for insulators); SEs are ideal for surface imaging [7, 10]. Biological and degradable samples that develop electrical charge from electron

beam incidence produce better imaging when insulated, given a conductive coating that is properly grounded to provide an electrical discharge path [7].

Employing CASINO to analyze the best methods for sample preparation and SEM parameters can be beneficial for biologists observing degradable organic biological samples, chemists in elemental analysis or identifying layers of compounds, and for engineers in the process of producing complex micro/nanostructures or integrated circuits [6, 7, 19, 20, 31-33].

2. Methods

Within CASINO 3V, utilizing the sample 3D designer capabilities, a new simulation was created with a sample that is modified to have the cylinder shape. The single cylinder shape represents the NF and is set with the chemical contents of PEI. The PEI NF sample was modeled and oriented in the x, y, z planes in the 3D space. The CASINO 3V, 3D space is designated with grid lines across the x, y, and z axis' in the model space. **Table 1 Simulation parameters of PEI, Al, and Au,** presents details of input parameters for the simulation. The chemical composition for PEI was input (density of 1.03g/cm^3, plasmon energy of 25eV, and work function of 3.5eV), with no layers, but separate layers and color designations are variable options that were selected for the compared sample preparation options. The diameter of all cylinders modeled for PEI NF have a 100nm radius with 20 divisions, for a total of 200nm diameter.

	Radius (nm)	Diameter (nm)	Cylinder	Length (nm)
PEI NF	100nm	200	20 divisions	800

	X dimension (nm)	Y dimension (nm)	Thickness is Density = in line with X Plane Density: 2.7g/cm^3 100nm to be below the fiber exactly
Aluminum (Al)	1000	1000	

	Density (g/cm^3)	Plasmon Energy (eV)	Work Function (eV)	From CASINO SE Database
PEI	1.03g/cm^3	25	3.5	N
Aluminum (Al)	2.7g/cm^3	15	4.28	Y
Gold (Au)	19.3g/cm^3	8.84	5.1	Y

220

221 **[Table 1. Simulation parameters of PEI, Al, and Au]** details of input parameters for the
222 CASINO 3V 3D simulations, including the modeling parameters (radius (nm), diameter (nm),
223 cylinder divisions, and length (nm)) for PEI NF, and dimensions (x and y) and thickness of Al, as
224 well as the density (g/cm^3), plasmon energy (eV), and work function (eV) of PEI, Al, and Au.

225

226 Also modeled for comparison in separate simulations was a grouping of 4 PEI NF, a PEI NF on
227 an aluminum sheet, and a gold coated PEI NF on an aluminum sheet. Each modeled sample was
228 simulated under a constant 100 electron emissions, with varying electron velocities to compare
229 the electron trajectories when exposed to the various preparation possibilities in order to
230 determine which would produce the incident beam electrons that create BSE and SE electron
231 pathways that are detectable for the best SEM visualization results.

232

233 Initially, a simulation was run on the single PEI NF model with an electron beam of 100
234 electrons emitted at 1keV - 30keV at increasing intervals of 5keV, to show the full PEI NF
235 sample independent from a coating, background, or base. Then 100 electrons were simulated
236 across a 3D modeled bundle of 4 PEI NFs, under the electron velocities of 1keV - 30keV at

increasing intervals of 5keV, independent from a coating, background, or base. This range, 1keV - 30keV, has been suggested as a stable beam velocity that can be utilized for longer periods of time on organic erodible sample types [7]. The 4 PEI NF bundle was modeled to enhance the visible electron interactions among the polymer sample, neighboring fiber surfaces as well as the penetrability of the electron paths through the NFs. The comparison of more material sample and electron acceleration voltage can be made. The simulation produced provides single PEI NF information on the electron incidence and escape. The simulations produced with 4 PEI NF samples, provides more PEI NF compounds in the target area of the beam for obtaining information on the electron incidence and escape, with a greater amount of sample for electrons to pass.

The PEI sample is composed of primarily carbon (C; Z 6) and nitrogen (N; Z 7), these elements have low Z that is conducive to charging, the higher the Z the lower the interaction volume is necessary for a given energy beam to produce a detective BSE and SE emissions. To reduce the sample charging for biodegradable materials in the SEM, preparations of conductive coatings and lowering of the beam energy are often done.

Simulations were continued to identify settings and sample preparation conditions (upon aluminum base and with a stain or coating) that are more optimal for the production of BSE and SE for SEM detection. The following simulations had the PEI NF sample set on a base of an Al sheet background. The Al (density 2.7g/cm^3; plasmon energy 15eV; work function 4.28eV) modeled had the dimensions of a 1000 x 1000 nm sheet with the plane directly below the sample, also in **Table 1**. To focus on the electron incidence upon the PEI NF sample on an aluminum

background, a single PEI NF on aluminum sheet was simulated under the electron velocities at 1keV - 30keV at increasing intervals of 5keV.

Metallic coatings upon biodegradable samples are often gold (Au; Z 79; density 19.3g/cm^3; plasmon energy 8.84eV; work function 5.1eV; in **Table 1**), due to its higher Z it induces more elastic scattering events with a broader distribution, lower sample penetration, and enhances SEM electron capture. This is also true for the choice of background chosen for the sample in which silver (Ag; Z 47) and Al (Z 13) are often utilized for because of the increased BSE per beam electron incidence [7, 34]. Au has greater electron beam resistance and less beam penetration depth, protecting the integrity of the structures to be visualized on the sample during the electron bombardment [7]. The high electron penetration, of low Z element containing samples, can also be prevented by setting the SEM to a lower electron beam energy. This is beneficial as the lower beam energies advents SE emissions, especially below 5keV [7].

To further enhance the electron escape trajectories, in addition to the Al background/base, the simulated single PEI NF was 3D modeled to have an Au layer, or coating, around the cylinder. This modeled sample preparation was simulated under the electron velocities of 1keV - 30keV at increasing intervals of 5keV.

Physical model settings selected for the aforementioned Casino 3V simulations were: Mott by equation (Browning (1994); Monsel) for total and partial cross section, lagged Fibonacci (Boost lf607) random number generator, Lowney (1994) Monsel for directing cousin, Joy and Lou + Lowney (Monsel) for dE/dS calculation, and Joy & Lou (1989) Monsel for ionization potential

[33, 35]. These specific settings were selected for inclusion of data, for the maximum capture of the generation of secondary electrons.

2.1 Electron Trajectory Output Defined

For optimal SEM imaging parameters, the desired electron scattering for this sample is low TE and AE with the depth of the electron paths redirecting within the sample with electron paths exiting the sample surface as the generated SE and BSE signals, with minimal primary electrons escaping the sample or becoming trapped within the sample causing charging. The measurements used for comparison are the electron responses of; inelastic (SE) or elastic scattering (BSE), the beam electrons energy and/or path being unchanged, the electron trajectory shape (advent of SE, BSE, or X-ray electrons), electron beam penetration, and escape from the sample.

It is not ideal to obtain highly **Absorbed** and **Transmitted Electrons**, because they are the electrons that have either been caught within the sample or have passed completely through the sample, respectively. **Absorbed electrons**, because they are the electrons that have been retained by the sample and are producing charges/changes through exciting ground state electrons within the sample to higher energy states, possibly causing pi transitions, molecular structure changes, molecular bond breaks, and conformational changes. Absorbed electrons are sought out in studies that query current and conductivity, such as in semiconductor device mapping. On an organic sample these changes damage the sample and distort the SEM imaging results.

Transmitted electrons pass through the specimen and darken the SEM image where the other electron signals (electron interactions and electron scattering; BSE & SE) are occurring, causing high contrast. A subset of TE is detected and CASINO 3V provides a prediction of the TE and the SEM detectable TE (dTE) particles captured. **Absorbed and Transmitted Electrons are not emitted (SE) or scatter (BSE) electrons.** SE and BSE are what is of interest for topography/morphology and composition/atomic number (Z) contrast, respectively. **SE** provides inelastic interactions with sample atoms, liberating/emitting electrons from the surface (5-50 nm) which produce SEM images with high-resolution of surface topography, texture, and morphology, a more 3D look. **BSE** provides elastic collisions with the sample's atoms, scattering from approx. 0.5–1μm within the sample which produce SEM images with phase separation, contrast, and composition (Z data; heavier elements appear brighter), a quality of 2D brightness. The desired result is to see high SE and BSE for the best quality of SEM imaging and data collection in an SEM setting. It is important to find the most suitable settings and preparation method for generation of both SE and BSE to reduce time using the SEM and gaining the most information from a small amount of disposed sample.

3. Results

As previously shown in the introduction, **Figure 1**, the CASINO 2V 2D simulation modeled the electron pathways through the sample, PEI NF on Al, but didn't provide enough information for practicable sample preparation for the SEM.

The following are the resulting figures (in tables) of the CASINO 3V 3D simulations developed to identify the sample preparation that best fits a biodegradable PEI NF sample for SEM. The simulation settings for all CASINO models will follow the color designation as in **Fig. 1**, which shows the color key of; TE/dTE (beam electrons) as yellow, BSE as red, SE as purple, dissipating energy electrons as green, and absorbed/X-Ray electron incidences as blue, from increasing to decreasing keV [17]. Each model is demarcated by the x, y and z grid of the 3D space and a keV color signature ranging from 0.00keV to the keV of the initial electron beam emission. Each simulation column will also have the numeration/designations of; asterisk symbol (*) for TE (dTE); caret symbol (^) for AE; obelisk symbol (†) for BSE; diesis symbol (‡) for SE, for that column's simulation. The distant view is approximately 300nm from the center of the model. The closer view is approximately 100nm from the center of the model. The side view (down the length of the cylinder) is approximately 100nm from the center of the model. The radial (down the cylinder NF center) view is approximately 100nm from the center of the model. A top impact (beam incident upon the NF from above) view at approximately 100nm from the center of the model is also represented. This color key figure applies to all CASINO model simulations and is also provided within the supplemental material as [**Supplementary Materials Figure 1. Electron Trajectory Color Key**] [18].

3.1 Electron Trajectories upon a single PEI NF

The build-up of charge that causes overt brightness that overpowers imaging (overheating), can be visualized in the **Table 2, CASINO 3V 3D simulation for single PEI NF under 100 electron beams at 1keV, 5keV, 10keV, & 30keV,** simulations, which shows numerically the

TE, dTE, and AE in the compared models. The beam fully penetrates the samples under 5-30keV beams (with high TE and dTEs), where at 1keV it does not, which had high AE of 255.3keV. High TE and dTE's are a signifier of contrast blocking of other electron path detection, and low AE signifies that there may be no atoms remaining for an electron to be interacted with and that the electrons are passing through, to be detected and added as high dTE, contributing to a brightness of the disorientating contrast. The 30keV is ruled out as an optimum setting for the sample, as the high keV is observed to negatively affect the sample in the SEM, though the simulations results of high TE, high dTE, low AE with high visible beam passage, and low advent of SE and BSEs. The results shown in **Table 2** indicate that none would be sufficient to produce a SEM image.

Table 2. CASINO 3V 3D **simulation for single PEI NF under 100 electron beams at 1keV, 5keV, 10keV, & 30keV.**

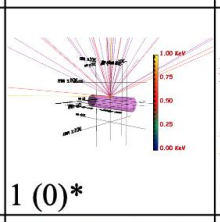
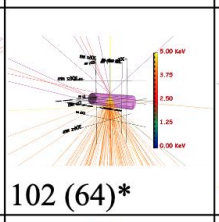
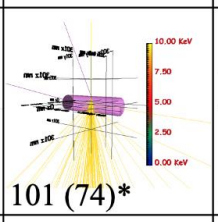
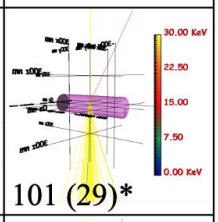
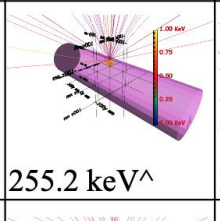
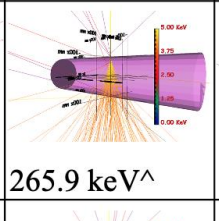
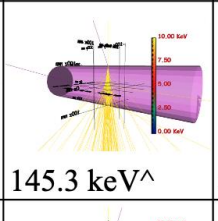
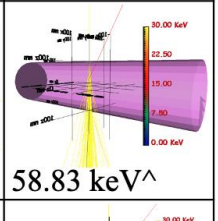
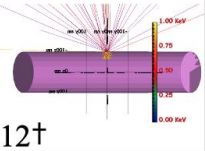
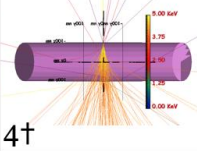
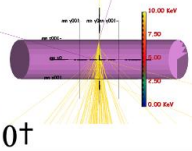
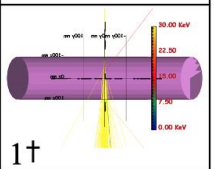
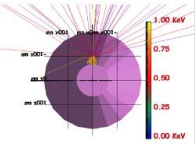
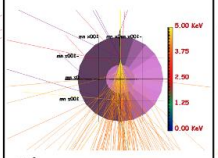
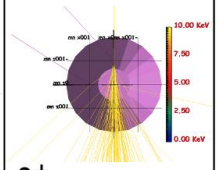
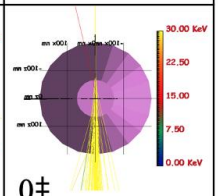
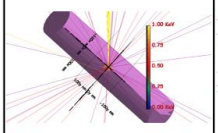
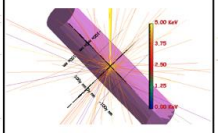
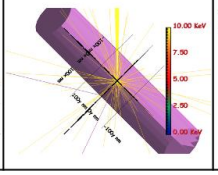
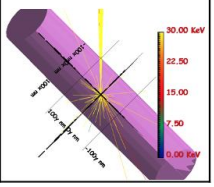
	Single PEI Nanofiber under 100 electron beam CASINO model			
	1 keV	**5 keV**	**10 keV**	**30 keV**
Distant View	 1 (0)*	 102 (64)*	 101 (74)*	 101 (29)*
Closer View	 255.2 keV^	 265.9 keV^	 145.3 keV^	 58.83 keV^
Side View	 12†	 4†	 0†	 1†
Radial View	 26‡	 6‡	 2‡	 0‡
Top Impact				

Table 2 shows a single PEI NF under 100 electron beams at 1keV, 5keV, 10keV, & 30keV.

3.2 Electron Trajectories of Differing keV upon Modeled Sample Types of Increased NF sample Number & Aluminum backed Sample

In **Table 3**, **CASINO 3V 3D simulation of 4 PEI NF & 1 PEI NF on Al under 100 electron beam at 1keV, 5keV, & 10keV, each,** the 1keV simulated beam upon the two sample types shows that the electron beam does not exit the sample through the opposite end. There is no full sample penetration of the beam under 1keV, and the low AE, are positive signifiers that there is not sample deterioration under the electron charge, and that the SE and BSE data can be obtained from an SEM and is not blocked by the dTE.

Table 3. CASINO 3V 3D simulation of 4 PEI NF & 1 PEI NF on Al under 100 electron beams at 1keV, 5keV, & 10keV, each.

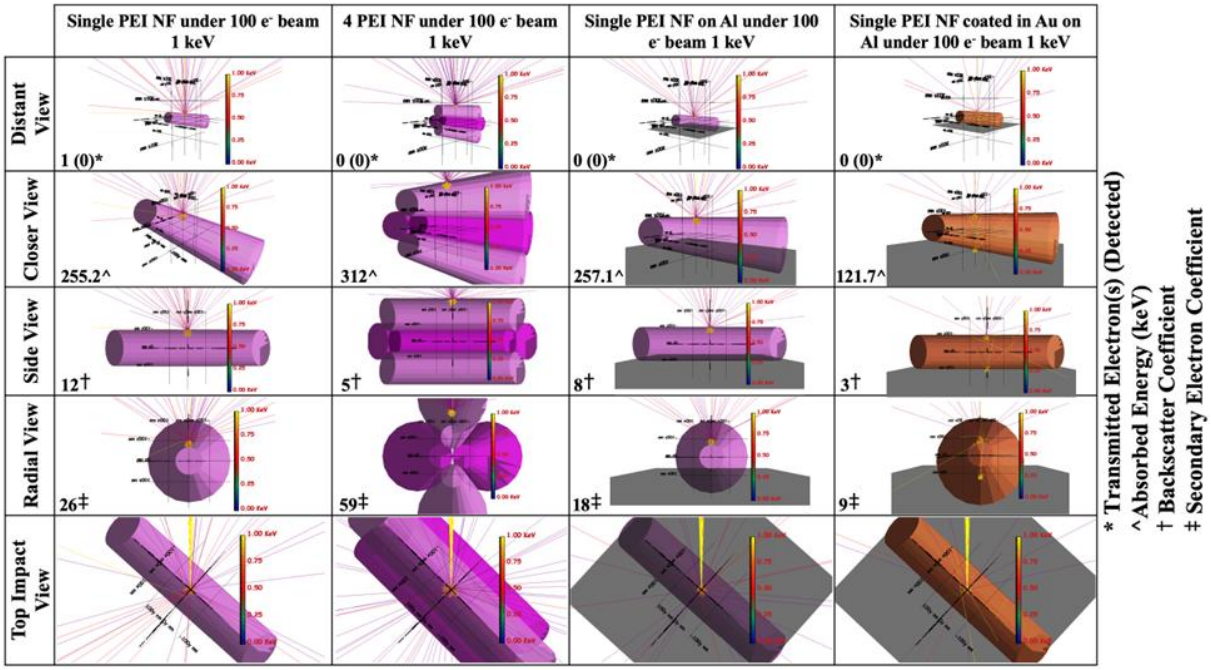
	4 PEI NF under 100 e⁻ beam 1 keV	4 PEI NF under 100 e⁻ beam 5 keV	4 PEI NF under 100 e⁻ beam 10 keV	Single PEI NF on Al under 100 e⁻ beam 1 keV	Single PEI NF on Al under 100 e⁻ beam 5 keV	Single PEI NF on Al under 100 e⁻ beam 10 keV
Distant View	0 (0)*	77 (25)*	96 (71)*	0 (0)*	2 (0)*	0 (0)*
Closer View	312^	900.9^	630.6^	257.1^	308.2^	157.7^
Side View	5†	9†	3†	8†	9†	11†
Radial View	59‡	24‡	17‡	18‡	7‡	5‡
Top Impact View						

Table 3 shows an electron beam of 100 electrons of the velocities of 1keV, 5keV, and 10keV, upon the sample preparations of 4 PEI NFs and 1PEI NF upon Al, each.

In **Table 3**, the 5keV and 10keV simulated beam incident upon the two sample types fully penetrate each sample. For the 4 PEI NF sample the electron paths show high signals of TE and dTE, with 77(25) at 5keV and 96(71) at 10keV. This is a signifier of contrast blocking of other electron path detections, like that predicted for the single PEI NF. the 4 PEI NF sample is indicating that at all keVs BSE and SEs will be produced but due to the high signals of TE and dTE their detection would be blocked. For the PEI NF/Al sample the electron paths show low signals of TE and dTE, with 2(0) at 5keV and 0(0) at 10keV. The keVs BSE and SEs detection would not be blocked by other detected electron paths. The 4 PEI NF sample with high AE at 5keV and 10keV indicate sample deterioration under the electron charge, with more sample available for absorption the AE is expected to be greater than the single NF samples. The AE is dampened with the PEI NF/Al or with using the lower keV beam charge on the sample. PEI NF/Al shows decreasing AE value with increased keV (at 1keV, 257.1 and at 10keV, 157.7) indicating that Al backing is lessening the absorption that causes sample damage. It is shown that the denser the sample size (4 PEI NF sample) the better the overall signal, but that a high TE, dTE, and AE does occur more with unprotected and not backed NF samples.

The10keV simulated beam incident upon the three sample types (**Table 2** and **Table 3**) fully penetrates each sample. The electron paths that are primarily TE and dTE for the models of PEI NF without Al, among which the single and 4 PEI NF samples show high signals of TE (dTE), at 101(74) and 96(71), **Table 2** and **Table 3** respectively. When comparing the single PEI NF to the 4 PEI NF, the sample preparations with more NF (4 PEI NF) show that with more fibers there is

418 greater BSEs (0 vs. 3 for 4 PEI NF; **Table 2** and **Table 3**) and more AE (145.3 vs. 630.6 for 4
419 PEI NF; **Table 2** and **Table 3**).
420
421 The lower keV beam charge on the samples have indicated the most reliable for producing BSE
422 and SEs with the least damage to the sample and SEM image blocking. In **Table 4**, **CASINO 3V**
423 **3D simulation results for single PEI NF, 4 PEI NF, single PEI NF on Al, and single Au**
424 **coated PEI NF on Al under 100 electron beam at 1keV**,the 1keV simulated beam incident
425 upon the four sample types' results (all except for the single Au coated PEI NF on Al (Au/PEI
426 NF/Al) were in the previous tables) show almost no TE and dTE for all of the samples,
427 signifying no blocking of other electron path detection.
428
429 **Table 4. CASINO 3V 3D simulation results for single PEI NF, 4 PEI NF, single PEI NF on**
430 **Al, and single Au coated PEI NF on Al under 100 electron beams at 1keV.**



431

Table 4. CASINO 3V 3D simulation results for single PEI NF, 4 PEI NF, single PEI NF on Al, and single Au coated PEI NF on Al under 100 electron beams at 1keV.

In **Table 4**, for all the sample types under 1keV, the SEs are greater than the BSEs, the Al and Au samples had reduced AE effecting the sample and TEs effecting the SEM image. The Au/PEI NF/Al was the most AE damage/deterioration protected with the low count of 121.7.

3.3 Comparison of Electron Trajectories of Differing keV upon Gold coated & Aluminum backed Model Sample

In **Table 5**, CASINO 3V 3D simulation results for Au/PEI NF/Al sample at 1 keV, 5 keV, and 10 keV. Each result for Au/PEI NF/Al sample is shown from the distant, closer, side, radial and from the top beam impact on sample views using an electron beam current of 100 electrons and accelerating voltages of 1keV, 5 keV, and 10keV. Table 5 shows results with the designations of: asterisk symbol (*) for TE (dTE); caret symbol (^) for AE; obelisk symbol (†) for BSE; diesis symbol (‡) for SE.

Table 5. CASINO 3V 3D simulation for single Au/PEI NF/Al sample under 100 electron beams at 1keV, 5keV, and 10keV.]

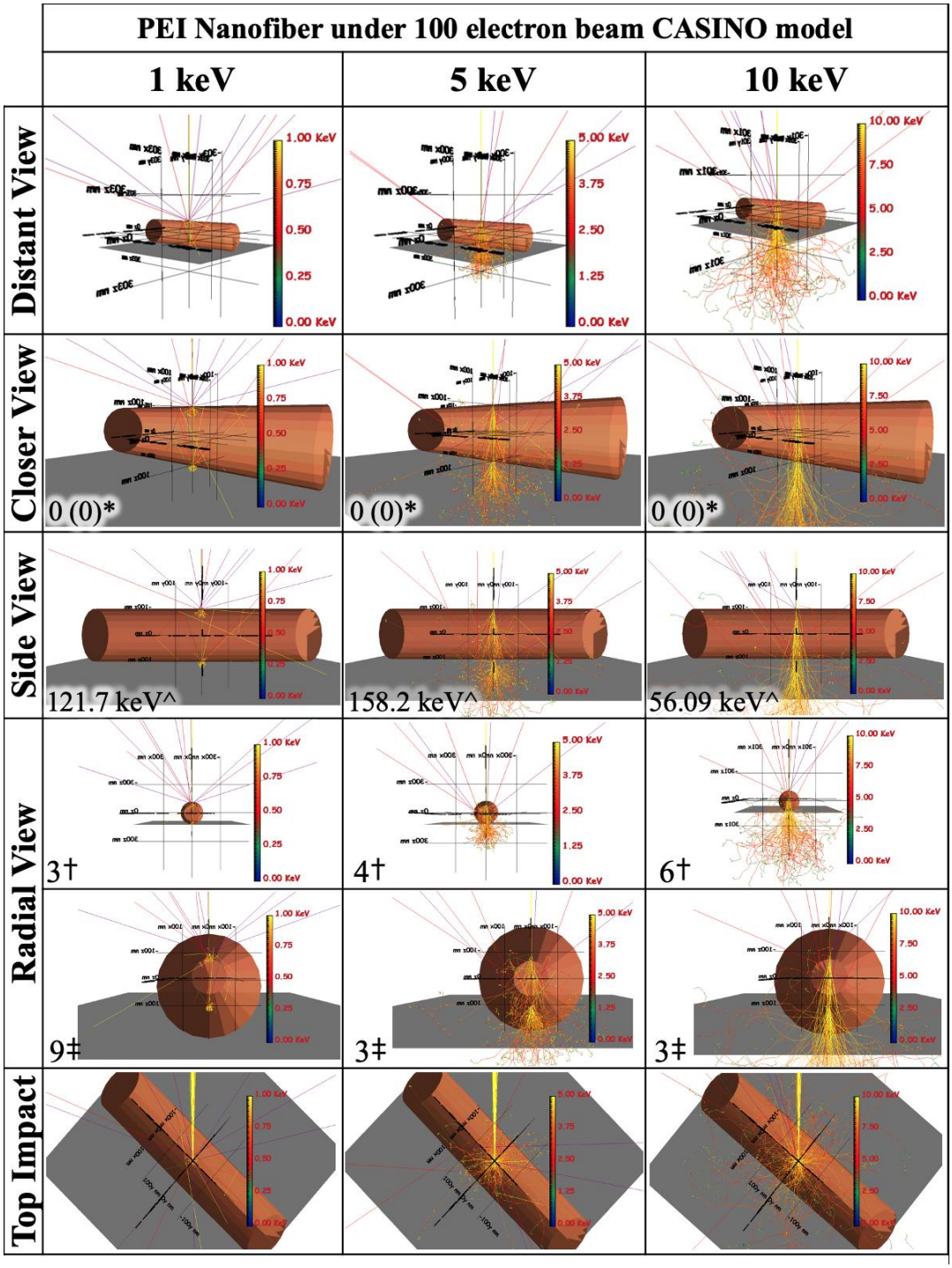


Table 5. CASINO version 3 (3D) simulations of Au/PEI NF/Al at 1keV, 5keV, and 10keV.

In **Table 5**, **CASINO 3V 3D simulation results for Au/PEI NF/Al sample under 100 electron beams at 1keV, 5keV, and 10keV**, there is complete primary electron penetration of the Au/PEI NF/Al at 5keV and 10keV, but not in the 1keV simulation, best visible in the radial, side, and distant views of the simulated samples. The Au/PEI NF/Al preparation method produced no TE and dTE. Au/PEI NF/Al at each keV resulted in AEs below 160, which is a good signifier of the PEI NF not having composition damage as much as those in previous simulated sample preparations, such as 630.6 for 4 PEI NF sample in **Table 3**.

Of the viewpoints, the radial, side, closer and distant views of each simulation, the electron paths at the edges of, and within, the sample are visible and can provide information about where the electron paths detected were generated from more clearly than the CASINO V2 2D simulation. As visibly evident within the Au/PEI NF/Al simulation results the 10keV maybe too strong to gain the information of the sample incidence and different features of the sample, vs the electron paths under the 1keV and 5keV beams which show separate electron interaction at the incidence of the Au coated NF and the Al. In the 5keV sample there is visual evidence of the possibility of obtaining electron trajectory data from the top of the NF sample as well as a separate detection of the Al backing, which could be significantly helpful for when more NF samples are used for the separate detection of each fiber from another. The 1keV shows such specific electron trajectories for the surface of the PEI NF on the top and bottom of the sample and is possibly the most ideal for obtaining the most accurate electron detection for scanning imaging. At the 1keV there is an advent of more BSE than SE and at the 10KeV there is an advent of more SE, which could be a choice made for the SEM user for which type of image information is preferred to obtain. The simulation comparisons of Au/PEI NF/Al support the assumption that the SEM parameters could

be distinguished from one another in the results and that those differences could reveal the advantages of different preparations of the sample.

Fig. 2 Absorbed Electron Beam Data, shows all of the modeled samples and SEM keVs simulated in this comparative study. It shows That PEI samples alone were taking on considerable AE, and with more of the sample the more energy absorption the sample can be inflicted with. This AE is damaging to the organic sample, but with Al as a base the sample materials are less effected by AE, especially above 5keV modeled simulations and Al is taking on the absorbed electron energy. The addition of an Au coating also decreased the AE that damages the PEI NF sample and takes on a little of the absorbed energy.

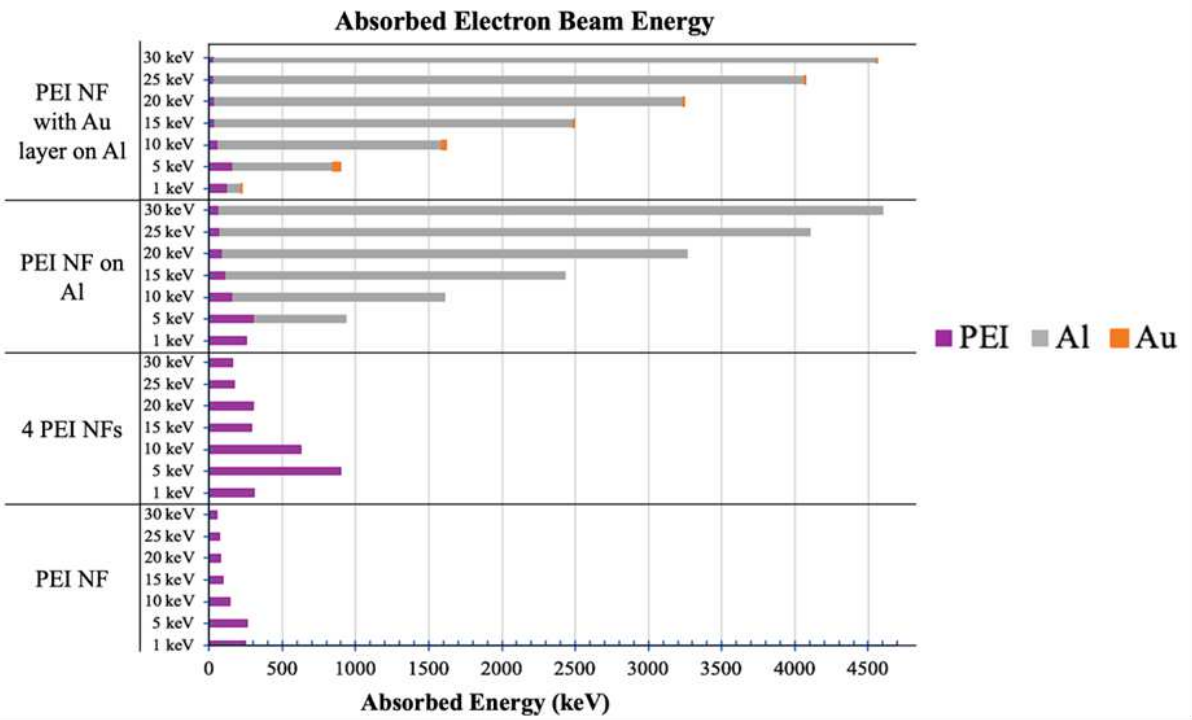


Fig. 2. Absorbed Electron Beam Energy

In all of the results, sample preparation on Al (simulation visuals in **Tables 4** and **Table 5**), there were significant SE and BSE produced, without the generation dTEs, which have the possibility to cause blockage of BSE and SE detection.

In **Fig. 3 Electron Distribution Data**, bar graphs present the SE (purple) and BSE (red) electron coefficients, and the scatter-dot line-connected plot presents TE (blue) and dTE (orange) electrons for all of the modeled samples of **1)** single PEI NF sample, **2)** 4 PEI NFs, **3)** PEI NF/Al, and **4)** Au/PEI NF/Al, and SEM keVs simulated in this comparative study. Each were simulated under electron beam of 100 electron trajectories at velocities of 1keV - 30keV at increasing intervals of 5keV (of a single sample point scan).

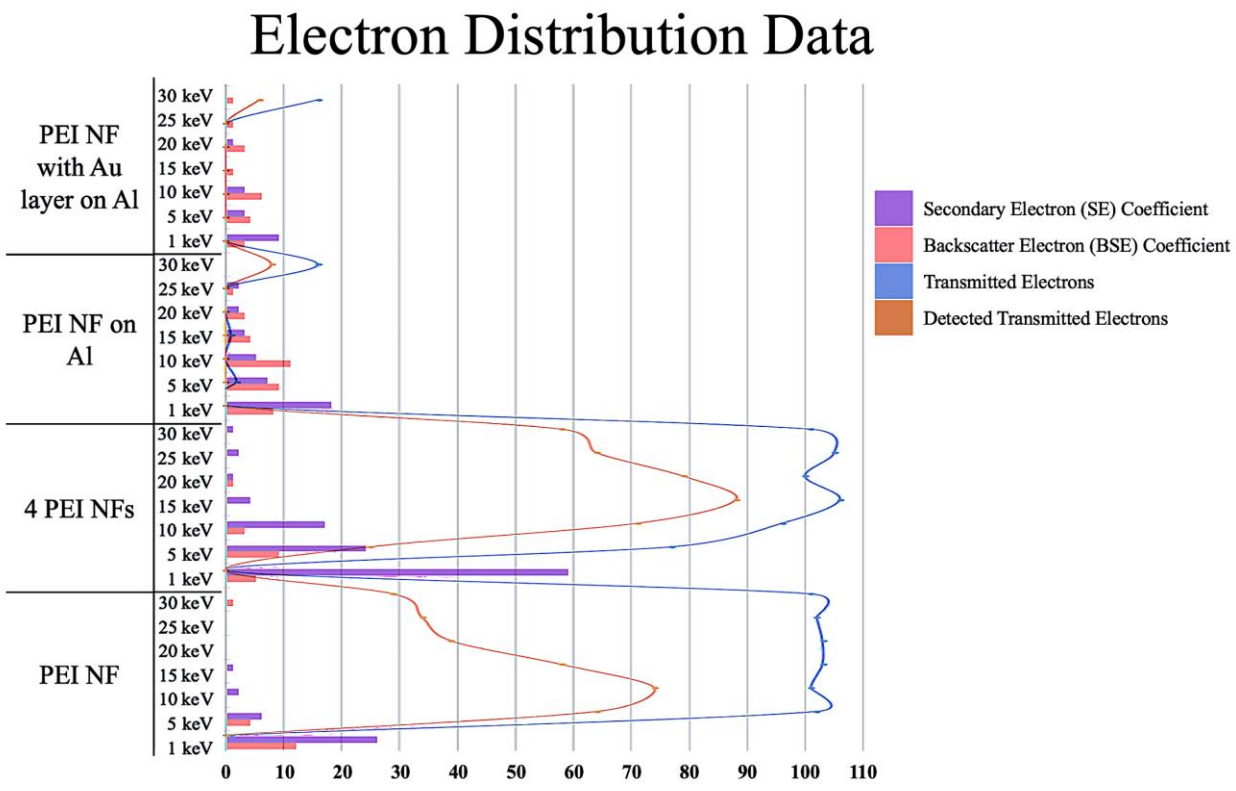


Fig. 3 Electron Distribution Data: SE, BSE, TE & dTE.

For the sample preparations of PEI NF and 4 PEI NFs there were high counts of TE and dTE, the dTE was the greatest between 20keV and 5keV, with the peak dTE's of 74 (10keV) and 88 (15keV), for PEI NF and 4 PEI NF respectively. The TE remained high for both of the modeled sample preparations at all voltages except for 1keV. TE for PEI NF all remained above 100 and for 4 PEI NF all counts remained above 75. The PEI NF/Al and Au/PEI NF/Al had TE and dTE counts below 2, with the exception of the simulations at 30keV, which produced 16 TE and 8 dTE and for Au/PEI NF/Al, 16 TE and 6 dTE. High dTE causes interference with the SEM detection of BSE and SEs, and for samples with Al base there was much less TE and dTE interference using electron voltages below 25keV.

BSE results for the 1keV PEI NF sample indicate low coefficients with 12 being the highest. Although this may indicate good contrast results the sample preparation is not as realistic with no base, which could also be said for the 4 PEI NF which had the highest BSE coefficient of 9 for the 5keV and 5 for the 1keV. This is the result that encourages using the lower 1keV and 5keV for this modeled sample type. The BSE coefficient results for PEI NF were 4 for the 5keV and 1 for the 30keV, the other simulations indicated 0 BSE coefficients. The BSE coefficient results for 4 PEI NF were 3 for 10keV and 1 for 20keV, the other simulations indicated 0 BSE coefficients. The overwhelming amount of TE and dTE that passed the samples PEI NF and 4PEI NF, with no Al base, could interfere with observing the BSE produced visual contrast, due to the high dTE that would translate to the visual representation as brightness. This enforces the theory behind the CASINO 3V simulations accuracy when observing the results of 0 BSE coefficients for the modeled samples of PEI NF at 10-25keV and for 4 PEI NF at 15keV, 25keV

and 30keV, because there may be none to detect with all of the electrons not impacting the sample for visual detection, but only transmitting through the SEM system.

BSE coefficients for the Al set samples were all above 0 except for that of the PEI NF/Al at 30keV. The 30keV simulated PEI NF/Al and Au/PEI NF/Al had low BSE (1 BSE coefficient for the later) but significant TE and dTE, which would not be ideal for SEM image translation due to the dTE brightness interfering with the contrast that the BSE coefficient detection provides. For PEI NF/Al the 15keV, 20keV and 25keV beam simulations had 4, 3, and 1 for BSE coefficients, respectively. For Au/PEI NF/Al the 15keV, 20keV and 25keV beam simulations had 1, 3, and 1 for BSE coefficients. For Au/PEI NF/Al the 1keV, 5keV and 10keV beam simulations had 3, 4, and 6 for BSE coefficients respectively, which are little better than the higher beam velocity (15keV, 20keV and 25keV) BSE results of PEI NF/Al. The best BSE coefficient results were that of the PEI NF/Al when simulated under 1keV, 5keV and 10keV, with beam velocities producing the coefficients of 8, 9, and 11, respectively. The BSE results for the samples modeled on Al produced the better coefficient counts when under the beam velocities between 25keV and 1keV. The difference between the two are that the PEI NF/Al produced higher BSE counts than that of the Au/PEI NF/Al, but the PEI NF/Al had more TE and dTE electrons that could impede the SEM translated visual image. Overall, the BSE coefficient results show favor for using the lower keV for producing the most BSE without dTE hinderance.

SEs, when detected are the producers of the SEM image topography, and the SE results show that all of the modeled sample types had higher SE coefficients at higher simulated electron beam exposures. The SE coefficient counts from beam simulations, 1-30keV in increments of

5keV, for PEI NF are: 26, 6, 2, 1, 0, 0, and 0. The SE coefficient counts from 1-30keV in increments of 5keV for 4 PEI NFs are: 59, 24, 17, 4, 1, 2, and 1. The SE coefficient counts from 1-30keV in increments of 5keV for PEI NF/Al are: 18, 7, 5, 3, 2, 2 and 0. The SE coefficient counts from 1-30keV in increments of 5keV for Au/PEI NF/Al on are: 9, 3, 3, 0, 1, 0, and 0.

In agreement with other CASINO utilized published works, there was decreased secondary coefficients as the electron beam keV increased [2, 7]. The SEs shallow escape depth (5-10nm) could be simulated and numerated for the predictions. In the SEM the preferential SE settings are lower keV electron velocities, under which the top 2-4 layers would be distinguishable from each other, and with the top layer being Au the visual detection maybe improved [2]. BSEs tend to increase as the electron beam keV increased in most literature, but for the PEI NF sample there was a marked increase of BSE detection at 10keV or lower, which provides deeper escape depths (1-5μm) for the electron paths that are detected. BSEs at the 1keV voltage were greater than at 10keV and higher (this is one of the reasons the higher keV values of 15-30keVs were not shown in the tables except for **Table 2**). The detection of SE and BSEs are predicted to be clearer within the SEM when the TE and dTE detection interference is reduced.

All of the above data is provided in **Supplementary Materials 2 CASINO PEI NF Simulation Data Table**.

4. Discussion

4.1 Comparison of Published Works

SEM instrumentation has improved for the purposes of what the simulations shown here confirm, with the advancement of focused low electron voltage beams and techniques to gain sample detail with preventative measures made to reduce sample damage [2]. Postek et al. (2020) describes brightness in the way that was described here as the TE and dTE interference, and in their publication they give a calculation for the accelerating voltage (Va) dictating the apparent brightness (B), which includes source emission brightness (Bc) and the amount of electrons of the initial beam (Ve) and that equation is [2]:

$$B = Bc \cdot \frac{Va}{Ve}$$

This equation can be used to support the evidence of low energies improving the generation of signal from shallower sample impact, secondary signal, and that at the higher energies there is reduced signal generation per the primary electrons. More specific equations can be obtained from Cuesta et al. (2022), of the operating principals behind laser amplified emission through an SEM and the electron density velocity upon the sample resulting brightness, along with other factors included within their calculations [18]. Baatsen el al. (2021) ran experiments on bioorganic materials to examine sample thickness and the resulting image resolution within the SEM. The carbon sample, mice cerebellum, sections shown clearer resolution with the highest accelerating voltage 1.5keV for a sample of 50nm thickness [30]. Although, as seen in the simulations shown here, the more sample size, that is NFs provided, the better the imaging there maybe, and an upper limit to that sample size may cause a decrease in resolution and a need to

alter the low voltage of electrons used to that of a slightly higher keV may provide better resolution.

The simulations conducted here further relate to the results of the Baatsen et al. studies in that at 10kV the structural details would become interfered upon by brightness, or as we refer to the TE and dTE, with the electron voltage accelerating the electrons to a depth of 1μm within the sample, which is well beyond that of the 100nm radii NF modeled within the simulations shown here. They also mention that at 100nm a 1μm depth could be penetrated by 2kV, which supports the simulation differences between using 1keV verses 5keV in the simulations, and the 5keV similarities to using the accelerating voltage of 10keV. They mention the image quality reduction when using 1.5kV upon 50nm sections as well. The simulations shown here highlight that between 5keV and 1keV the reduced TE and dTE (brightness) may provide the best resolution image. Within the Baatsen et al. image quality breakdown studies, in the cases of 100nm sample section sizes they found that at the keV between 1.5 and 3 provided quality imaging. The CASINO 3V simulations shown here on the NF 100 radii sample would support that finding. The Baatsen et al. of 200nm is the most similar to the simulations shown here with their 200nm sample section, and the PEI NF sample diameter being 200nm, their result for 1.5kV and 2kV were high contrast images, this relates to the high values that were obtained here for BSE, without TE and dTE conflict. At the 300nm sections of the Baaatsen et al. samples, which would related to the multi NF samples simulated the result of quality images could be obtained at a greater range, 1.5-3kV, without deterioration, which the simulations confirm [30].

The observed CASINO 3V simulation results here are in agreement of what Mussakhanov et al. (2024) observed in their studies on water/cerium-activated yttrium Al garnet ceramic samples for charge on the samples media absorption capacity. Within their experiments they observed the generation of SEs when using the SEM and describe the events as electrons from the beam penetrating the sample material scattering the atoms, causing energizing and ionization of the sample elements as the electron paths pass through and not only pass through but to transfer the energy to the sample. The energy transferred to the sample from the electron beam is absorbed, it reaches a maximum capacity within the sample matter before decreasing. The depth the electron path reaches within the sample and distribution of energy loss, depend on the beam energy and the electron beam width. In the simulations that were conducted here the beam width remained unchanged. Mussakhanov et al. utilized the CASINO 2.5V in their modeling methodologies and include an equation for inelastic scattering and energy loss in addition to the software's elastic collisions that fit a Gaussian flux distribution. [36]

For all of the above compared studies they have each come to the same conclusion of thin or nanometer samples requiring low accelerating voltages, to produce both BSEs and SEs. Emission intensity and penetration depth was not compared but could be compared with further extrapolation of the data and compared with the Cuesta et al. results of the emission intensity being a function of penetration depth, as well. The range of 0.5keV was not compared as the software indicated this as a weak computing area, but for future examination could be tested in a simulation for accuracy to be a pre-SEM simulation method protocol for mass jobs. In a true macro environment, the scenario of a single NF being hit with an electron beam and identified by a SEM user is highly unlikely, but for complete understanding of the electron pathways, the

comparison of a single verse a NF grouping, with no backing, was revealing for more accurate beam velocity effects to choose.

5. Conclusion and Future Directions

There is a variety of possibilities for electron beam trajectories to traverse solids and their applications. CASINO 3V software can be used to not only narrow the quantitative range of SEM settings to utilize, but to define better preparation tactics for your solid of interest to get the best quality result. Sample bombardment can occur when the methods of sample preparation are not fully examined before approaching the SEM. Not only could the sample of interest become damaged and unrecognizable but the reaction of the sample to the electron beam could damage the costly and valuable SEM sample chamber and microscope. Properly preparing the sample for the electrical charge that is it develops during the electron beam impact, is a part of the necessary grounding for the electrical discharge of the electron path. The more that the electron path is provided a clear path trajectory the clearer the emissions and scatter results will be, which provide the better visual results. This is the reason that conductive coating, and base setting is an important preparation step in the pre-SEM process. [7]

This project aimed at simulating, identifying, and proving the reasoning behind the SEM range predicted to use by the simulations and the sample preparations to use, that is suitable for getting an SEM image of a degradable organic sample. This process shows a method of comparative simulations in CASINO 3V that can be used for other samples and purposes such as, defining and showing the electron beam dissipation for electron beams used in medical device

applications or sterilization, defining beam depth of electron beam products or cutting devices, for the use of enhancing microscopy methods for the engineering of circuit design, and for predicting the amounts of absorbed energy during the passage of electron voltage flow through the samples matter. [36]

The goals of the project is to identify the sample preparation and SEM parameters for the greatest advent and detection of inelastic scattering electrons (secondary electrons; SEs), for sample topography details, and elastic scattering (backscatter electrons; BSEs), for composition and contrast sample details. Using CASINO 3V the biodegradable PEI NF, with cross-section of 200nm, was compared in visual 3D models under conditions of a single PEI NF, bundled sample (4 PEI NF), on an Al base and on an Al base coated in Au, under a 100 electron beam at varying voltages between 1keV to 30keV.

The polymer sample chosen, PEI/B-PEI, is non-conductive, biodegradable ($(C_2H_5N)_n$), and prone to deterioration of up to 10nm, when electron incidence charge builds up, this build up is evident in many of the simulations in which the beam electrons (yellow) penetrate through the entire sample. The voltages of 10 and 30keV deteriorate the initial 4 PEI NF simulations, and the higher electron voltages did not produce significant electrons for sample detection, but for the 4 PEI NF sample the 5keV had significant BSEs. BSEs (red) are from electron collisions with the sample elements atomic nuclei, which also releases X-ray photons (blue) with an element-specific energy, and when detected gives atomic number/phase contrast information [3-7, 10, 20, 31]. Ideally the simulation would show all of the colors in the electron trajectory key, with the SEs (purple) and BSEs (red), providing detection of topographical and contrast of the sample.

This was obtained when the sample was modeled to have an Au coating and Al base. Au coating the has been a technique for SEM NF sample prep. When simulating a single, Au coated PEI NF the electron beam incidence is seen on the surface of the NF (top and bottom) in the images of simulations at 1keV and 5keV separating the signals of the NF and the Al sheet. At both 1keV and 5keV the NF and Al surface signals can be distinguished and give way to better topographical information of the sample, through SE generation detection. Au coating protects the sample and gives way to better BSE detection than a lower atomic number (Z) atoms at higher electron beam voltages. In the data shown, the best parameters were that of the sample preparations on Al with Au coating under a 100 electron beam, specifically; at 10keV for only BSE detection, 5keV for both BSE and SE detection and 1keV for the best detection of SEs. The inclusion of higher atomic value materials provided biodegradation protection, reduced the production of TE and dTE that formed brightness upon an SEM image and allowed for more elastic scattering at the higher electron beam voltages, which provided focused electron trajectories upon the sample material.

Materials with higher atomic numbers (Au and Al) exhibit stronger elastic scattering, BSEs. This increased scattering rate, limits the penetration depth (TE), and lateral spread of the electron trajectories (dTE) compared to lower atomic number materials, such as C, N, and O. The lateral spreading of electron trajectories due to multiple elastic scattering events means that signals can originate more from the sample, from the initial beams impact point. With the higher TE and dTE it was evident that their effects can limit the special resolution possible. [3-5]

With greater signals of both BSEs and SEs further sample information can be obtained by the eventual X-Ray emissions for energy-dispersive spectroscopy (EDS.) SEs generated inelastically leave electron vacancies that are sometimes filled producing an X-ray emission and BSEs elastic scattering excites inner shell electrons to emit X-rays. X-ray advent is of interest to further be used for sample examination that can be done by EDS, immediately following SEM, to provide qualitative and quantitative analysis on the sample's elements. Sample preparation adaptions to compensate for the sample destruction within SEM, will also enhance the generation of X-ray electron advent for EDS elemental analysis. [7] CASINO uses the Monte Carlo calculation simulation and records the exit energy of each electron, and from this data the energy distribution of the electron's trajectories can be calculated. Casino 2V provided an X-ray emission spectrum that the 3V didn't. [7]

The CASINO analysis can continue to be followed up with in defining the keV and sample preparations to produce maximum X-ray electron incidences, to optimize the microscopic elemental detail capture. X-ray generation requires the velocity of the electron from the beam to be equal to, or have higher, velocity of the orbiting electrons within the sample. The incoming electron ionizes a sample atomic shell electron causing it to leave the sample. [7]

X-ray emissions for EDS detection of atomic number were not discussed throughout this article due to the beam settings requiring more electron beam velocity applied to gain atomic number quanta from the electron detected trajectory, identify the optimal parameters can be looked into, with this study's base information on optimal SE and BSE advent for this sample type, sample size, preparation method and parameters. [7] It is predicted that more X-ray emissions and detection can occur for biodegradable or NF samples with a quick burst of 30 keV for providing

more x-ray photon detection for EDS and is recommended to do after obtaining an optimal SEM image at the lower SEM keV settings range that were identified as optimal in this study.

This pre-SEM simulation methods is significant for the purpose of limiting the electron beam damage to the sample in the goals of using EDS and X-Ray as well post imaging for information on identifying the chemical composition. Chemical composition analysis in the further analysis can be compared to the pre- and post-resulting sample to define the content of the sample that may have been damaged or degraded during the SEM analysis to obtain a relationship between your sample degradation and the amount of absorption that occurred during the SEM use. Future directions will be able to use the CASINO simulation validated parameters to then implement the preparation needs and parameters, upon actual samples under the same conditions within the SEM and compare the results produced, if they coincide accurately then better preparation can be done prior to using the SEM moving forward.

5.1 Other Methods to Obtaining Better Resolution SEM at Low Voltage for Organic Samples

For non-conductive samples, deep penetration at high keV creates charge and decreases image quality (like the NF alone or NF on Al sheet). For conductive samples or sample preparing adaptions, like the Au coated NF on Al, small wavelength/ higher keV can be used for increased resolution and damages sample less. The beam size can be altered but it is preferred to be small for better area resolution. In the future, to simulate the entire surface of the NF under the same optimal scanning of that beam, the beam size can be increased to cover more surface area of the sample, gaining a fuller spread of the NF topography with angling of the sample to the beam as

an option also. Reduce material damage and increase detection of BSE and SE for imaging may require mounting the sample on a heat sink/thermal management or using pulsed excitation. [10, 18]

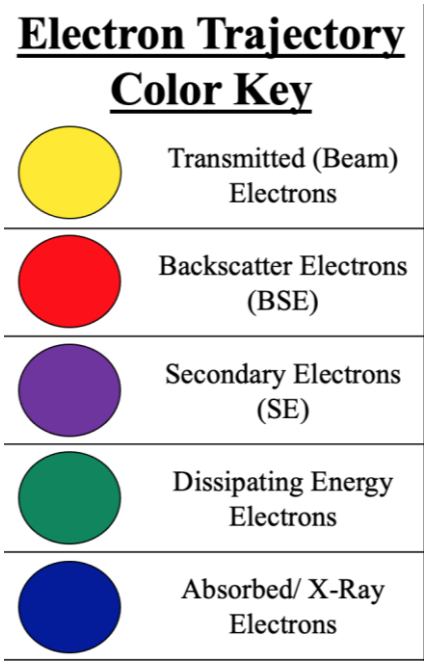
If the sample cannot be coated variable pressures in the sample chamber could be applied as a low pressure to reduce charging effects from TE, dTE and electron backscatter diffraction (EBSD)" (Goldstein) Another SEM variable to note in pre-SEM preparations is the pressure that occurs within the sample chamber, which can range from 1Pa to 2000Pa (not a variable changed in this study but highly worth noting) that it is a setting that may be altered within the SEM and CASINO software model and for an organic sample may improve results if in the range of 10–20 Pa. [7] Also within CASINO to model is that the tilt capability of the sample base within the SEM chamber was not compared or altered. Adaptions to the tilt of the sample base within the SEM chamber would improve the electron incidence scatter and capture as it provides more surface area for the single beam to spread upon collision and has shown evidence of increasing SE and BSE capture within area of incidence and depth. [7]

Graphed/plot data from CASINO 3V was utilized and adapted in this study but not necessarily needed for the interpretation and confirmation of parameters to identify a samples optimum SEM setting and preparation to begin with in SEM, because the visual confirmations of electron path to sample penetration using CASINO may suffice and are shown to be accurate with the related CASINO used publications mentioned within the results and discussion. For the more defined parameters to conserve the sample following up as was shown here, with comparisons and plots,

780 which provide a clearer view of what may be being exchanged in the alterations of velocity and
781 sample preparation.
782
783 The purpose of this project is to share a sample preparation process that can be utilized by
784 chemists, engineers and biologist when approaching the use of a SEM microscope with an
785 organic or degradable sample by first conducting simulations upon their modeled samples with
786 varying settings to identify the settings that are the most suitable for electron detection and
787 preservation of the sample. The goal of the process shown was to identify, through the CASINO
788 3V simulation model, what sample preparations that are the best fit for the improved
789 visualization through SEM, and sample preservation, of PEI NF sample. The CASINO
790 simulation can be used to estimate the SEM electron penetration depth into a polymer NF
791 sample. The penetration depth of electrons into the sample is dependent upon the elemental
792 composition of the sample and the acceleration-voltage of the electron beam. Valuable and
793 accurate predictions can be obtained through CASINO simulations to predict SEM electron
794 output before SEM voltage bombardment of real samples to obtain more accurate parameters for
795 voltage electron beam values and sample preparation. [6, 7, 20, 31]
796
797 Monte Carlo simulation programs like CASINO provide fundamental insights into electron-
798 sample interactions, which are essential for optimizing both the preparation of samples and the
799 operating parameters of the SEM for specific applications across biology, chemistry, and
800 engineering. [16] This is particularly valuable when dealing with challenging samples such as
801 beam-sensitive organic materials, complex layered structures, insulating specimens, or nanoscale
802 features.

6. Supplementary Material

Supplementary Material Fig. 1 Electron Trajectory Color Key



In **Supplementary Material Fig. 1 Electron Trajectory Color Key**, shows the color reference guide to the colors shown in the CASINO 2V and 3V software for the various electron trajectories. Electron trajectory keV are color designated electron beams; initial transmitted beam electron trajectories (yellow), backscatter electrons (BSE; red), secondary electrons (SE; purple), dissipating energy electrons (green) and X-Ray electron incidences (blue; indicate absorbed electrons), from increasing to decreasing keV [2, 18].

Supplementary Material Table 1. CASINO PEI NF Simulation Data Table

Model	e^- Beam Voltage	Absorbed Energy (keV)				BSE Coefficient			SE Coefficient			Trans-mitted Electron (s) (Detected)
		PEI	Al	Au	Sum	PEI	Al	Au	PEI	Al	Au	
PEI NF	1keV	255.2	-	-	255.2	12	-	-	26	-	-	1 (0)
PEI NF	5keV	265.9	-	-	265.9	4	-	-	6	-	-	102 (64)
PEI NF	10keV	145.3	-	-	145.3	0	-	-	2	-	-	101 (74)
PEI NF	15keV	101.9	-	-	101.9	0	-	-	1	-	-	103 (58)
PEI NF	20keV	83.16	-	-	83.16	0	-	-	0	-	-	103 (39)
PEI NF	25keV	76.18	-	-	76.18	0	-	-	0	-	-	102 (34)
PEI NF	30keV	58.83	-	-	58.83	1	-	-	0	-	-	101 (29)
4 PEI NFs	1keV	312	-	-	312	5	-	-	59	-	-	0 (0)
4 PEI NFs	5keV	900.9	-	-	900.9	9	-	-	24	-	-	77 (25)
4 PEI NFs	10keV	630.6	-	-	630.6	3	-	-	17	-	-	96 (71)
4 PEI NFs	15keV	292.4	-	-	292.4	0	-	-	4	-	-	106 (88)
4 PEI NFs	20keV	307	-	-	307	1	-	-	1	-	-	100 (79)
4 PEI NFs	25keV	173.9	-	-	173.9	0	-	-	2	-	-	105 (64)
4 PEI NFs	30keV	162.8	-	-	162.8	0	-	-	1	-	-	101 (58)
PEI NF on Al	1keV	257.1	0	-	257.1	8	X	-	18	X	-	0 (0)
PEI NF on Al	5keV	308.2	629.4	-	937.6	9	X	-	7	X	-	2 (0)
PEI NF on Al	10keV	157.7	1456	-	1614	11	X	-	5	X	-	0 (0)
PEI NF on Al	15keV	109.4	2327	-	2436	4	X	-	3	X	-	1 (0)
PEI NF on Al	20keV	88.73	3179	-	3268	3	X	-	2	X	-	0 (0)
PEI NF on Al	25keV	69.34	4037	-	4106	1	X	-	2	X	-	0 (0)
PEI NF on Al	30keV	62.15	4544	-	4606	0	X	-	0	X	-	16 (8)
PEI NF with Au layer on Al	1keV	121.7	97.57	5.364	224.6	3	X	X	9	X	X	0 (0)
PEI NF with Au layer on Al	5keV	158.2	688.1	51.06	897.3	4	X	X	3	X	X	0 (0)
PEI NF with Au layer on Al	10keV	56.09	1534	29.55	1620	6	X	X	3	X	X	0 (0)
PEI NF with Au layer on Al	15keV	35.55	2450	0.428	2485	1	X	X	0	X	X	0 (0)
PEI NF with Au layer on Al	20keV	35.79	3203	0.4575	3239	3	X	X	1	X	X	0 (0)
PEI NF with Au layer on Al	25keV	26.45	4039	3.463	4069	1	X	X	0	X	X	0 (0)
PEI NF with Au layer on Al	30keV	26.31	4528	0.2965	4555	1	X	X	0	X	X	16 (6)

PEI = Polyethylenimine Au = Gold T = Top
NF = Nanofiber B =Bottom - = Not applicable for tested model
Al Aluminum I = Infinate X = same for all elements

816

817 The **Supplementary Material Table 1. CASINO PEI NF Simulation Data Table,** shows the
818 numerical results of Absorbed Energy (in keV for each molecule in the sample PEI, Al, and Au
819 along with the sum of them combined), backscatter electron emission coefficient (for each

molecule in the sample PEI, Al, and Au), secondary electron coefficient (for each molecule in the sample PEI, Al, and Au), Transmitted Electrons and detected transmitted electrons from the CASINO 3V 3D simulations run on the samples PEI NF, 4 PEI NFs, PEI NF on Al, and PEI NF with Au layer on Al, at 1keV, 5keV, 10keV, 15keV, 20keV, 25keV, and 30keV electron beam velocities each.

7. Declarations

7.1 Data Availability

The data set (above) in the Supplemental Material titled "CASINO PEI NF Simulation Data Table" is the entire data set which the conclusions of the manuscript were based upon. The dataset supporting the conclusions of this article is included within the article as an additional file, in the Supplemental Material titled "CASINO PEI NF Simulation Data Table".

7.2 Authors Affiliations (COI)

[1] **Brandi J. Cook, MS (Primary/ Corresponding Author)**; No conflict of interest to declare.
PhD Candidate in the Department of Chemistry, College of Arts and Sciences, University of South Florida, Tampa, FL, USA
Master's degree in Cellular Biology, Microbiology and Molecular biology (CMMB) from Department of CMMB, College of Arts and Sciences, University of South Florida, Tampa, FL, USA

Bachelor of Science in Microbiology with emphasis in Chemistry from the College of Arts and Sciences, University of Montana, Missoula Mt. USA

Bachelor of Arts in Cellular and Molecular Biology from the College of Arts and Sciences, University of Montana, Missoula Mt. USA

Affiliations: Studied microscopy and histology technician training courses at Merritt Community College, in Oakland, California. Volunteered as a medical equipment sorter at the non-profit organization, MedShare, which collects unused medical equipment from U.S. hospitals and sends them with medical teams to developing countries in need.

[2] **Wayne C. Guida, PhD**; No conflict of interest to declare. Department of Chemistry, College of Arts and Sciences, University of South Florida, Tampa, FL, USA

Professor in the Department of Chemistry, University of South Florida in Tampa and Professor in the Drug Discovery Program at the H. Lee Moffitt Cancer Center & Research Institute at the University of South Florida.

Affiliations: Prior to coming to USF/Moffitt, Dr. Guida served as President and CEO of Schrödinger, Inc. and continues to serve on the company's Scientific Advisory Board.Prior to his role as CEO of Schrödinger, he was Executive Director of Biomolecular Structure, Lead Finding, and Computing at the Novartis Institute for Biomedical Research (formerly CIBA-Geigy Pharmaceuticals) in Summit, New Jersey, where he supervised a group of scientists engaged in molecular modeling, structural bioinformatics, X-ray crystallography, protein NMR spectroscopy, protein biochemistry, and high-throughput screening. His work

at CIBA-Geigy, along with collaborators at the University of Alabama at Birmingham, Southern Research Institute and BioCryst Pharmaceuticals, resulted in one of the first successful examples of the use of Structure-Based Drug Design in drug discovery.That work led to the development of clinically tested inhibitors of purine nucleoside phosphorylase.Prior to joining CIBA-Geigy, Dr. Guida was one of the original developers of the MacroModel program at Columbia University.

Dr. Guida's main research interests include the design of inhibitors of enzymes in signal transduction pathways and the biosynthetic pathways of polyamines and lipids.These inhibitors have potential utility as drugs for the treatment of cancer and infectious diseases.The discovery, design and synthesis of non-covalent, copper-based 20S proteasome inhibitors for the treatment of cancer is also an area of significant interest to Dr. Guida's group.

[3] **Sylvia W. Thomas, PhD**; No conflict of interest to declare. Department of Electrical Engineering, College of Engineering, University of South Florida, Tampa, FL, USA

Associate Professor & V.P. of Research & Innovation, University of South Florida
Fellow, American Institute for Medical and Biological Engineering
Senior Member, National Academy of Inventors

Dr. Sylvia Wilson Thomas is an Associate Professor in Electrical Engineering, affiliate faculty in Medical Engineering, and former Assistant Dean (Engineering) at the University of South Florida (USF) College of Engineering in Tampa, Florida. Associate Professor in Electrical Engineering and former Assistant Dean for the College of Engineering at the

University of South Florida leads the Advanced Materials Bio and Integration Research (AMBIR) laboratory at USF.

Affiliations: Dr. Thomas, the V.P. of USF's Research & Innovation, leads the Advanced Membrane and Materials Bio and Integration Research (AMBIR) laboratory at USF. Dr. Thomas' research and teaching endeavors are focused on the investigation of bio (biomedical, biological) and nano electronic device integration using advanced material systems for nano membrane technology, energy harvesting, sustainable environments, drug delivery, and bio-applications to meet global technological challenges. She also conducts research on the diversity, equity and inclusion of under-represented minorities and women. Her research has been funded by more than $4.8M and 12 patents/patent disclosures. She has directly mentored over 150 students as major/co-major professor (12 PhDs, 10 MS), committee member (50 PhD/MS), REU mentor (over 90 undergraduates, inclusive of role as NSF REU PI, 3 Senior Design projects and 1 Honors Thesis), and RET mentor (30 teachers, inclusive of role as NSF RET CoPI). She has also fostered and been engaged in collaborations and engineering education efforts in Italy, Puerto Rico, Singapore, Portugal, South Korea, Mexico, and South Africa. Dr. Thomas is a fellow of the National Academy of Inventors and a fellow of the American Institute for Medical and Biological Engineering.

7.3 Author Contributions & Acknowledgements

Brandi Cook (primary/ corresponding author) designed the study, performed the tests, analyzed the data, wrote the first draft, and implemented final text after all authors reviewed the final text. Dr. Thomas, co-Professor Investigator (co-PI) roles in conceptualization, funding acquisition, supervision, project administration, critical manuscript revision, and reviewed the final text. Dr. Guida, co-Professor Investigator (co-PI) roles in conceptualization, supervision, project administration, and reviewed the final text.

Acknowledgements go out to the Nanotechnology Research and Education Center (NREC) of the College of Engineering at USF staff for introduction to the CASINO software and SEM through their dedicated and considerate staff Sclafani Louis-Jeune, Dr. Jay Bieber, Dr. Yusuf Emirov and Robert Tufts.

7.4 Funding & Competing Interests

This work was supported by the National Science Foundation IRES BEAMS (Grant No. 1952589), for the training at NREC (Nanotechnology Research and Education Center) for graduate student researchers within the Advanced Materials Bio and Integration Research (AMBIR) laboratory.

7.5 Clinical Trial & Ethics Statement

There were no clinical trials. This is a computational chemistry study on a modeled nano sample. There are no ethics, consent to participate, and consent to publish declarations necessary to submit, as the work reports research involving computational chemistry study on a modeled nano sample with no human or animal subjects, their data and biological materials.

8. References

1. Zhao M, Ming B, Kim J-W et al (2015) New insights into subsurface imaging of carbon nanotubes in polymer composites via scanning electron microscopy. Nanotechnology 26(8):085703. doi:10.1088/0957-4484/26/8/085703
2. Postek MT, Vladár AE, Poster DL et al (2020) Ultra-low landing energy scanning electron microscopy for nanoengineering applications and metrology. Nanoengineering: Fabrication, Properties, Optics, Thin Films, and Devices XVII: SPIE, 77-85. doi: 10.1117/12.2567051
3. Jensen W (2022) Interpreting images from scanning electron microscopy. In: Resources: Tech Briefs 026. Available via Deringe-Ney. https://deringerney.com/interpreting-images-from-scanning-electron-microscopy/. Accessed 8 Mar 2022
4. Callister WD Jr (2000) Materials science and engineering-an introduction. Anti-Corrosion Methods and Materials. 47(7). John Wiley & Sons, Inc, New York, NY

5. Gauvin R, Lifshin E, Demers H et al (2006) Win X-ray: A new Monte Carlo program that computes X-ray spectra obtained with a scanning electron microscope. Microscopy and Microanalysis 12(1):49-64. doi:10.1002/sca.20262

6. Demers H, Poirier-Demers N, Couture AR et al (2011) Three-dimensional electron microscopy simulation with the CASINO Monte Carlo software. Scanning 33(3):135-146. doi:10.1002/sca.20262

7. Goldstein JI, Newbury DE, Michael JR et al (2018) Electron Beam-Specimen Interactions: Interaction Volume. Scanning Electron Microscopy and X-Ray Microanalysis. New York, NY: Springer New York, pp 1-14. doi: 10.1007/978-1-4939-6676-9

8. Needs RJ, Towler, MD, Drummond ND et al (2004) CASINO version 1.7 User Manual, University of Cambridge, Cambridge.

9. Joly D, Poirier-Demers N, Demers H (2011) Casino 3.2 User Manual. Universite de Université Sherbrooke, Québec, Canada

10. Hunt MS (2019) Scanning Electron Microscopy (SEM) Concepts. In: SEM diagrams handout (concepts). The Kavli Nanoscience Institute at Caltech. Available via Caltech. https://bit.ly/31bAyv8, Accessed 30 Mar 2025

11. Needs R, Towler M, Drummond N et al (2019c) Users Guide Version 2.13 (2022). University of Cambridge, Cambridge

12. Needs R, Towler M, Drummond N et al (2019b) Users Guide Version 2.13 (2015). University of Cambridge, Cambridge

13. Needs R, Towler M, Drummond N et al (2019a) Users Guide Version 2.13 (2013). University of Cambridge, Cambridge

14. Towler M (2000) An introductory guide to Gaussian basis sets in solid-state electronic structure calculations. European Summer School "Ab initio modelling in solid-state chemistry" Turino. University of Cambridge, Cambridge
15. Towler MD (2011) Quantum Monte Carlo, or, how to solve the many-particle Schrödinger equation accurately whilst retaining favourable scaling with system size. Computational Methods for Large Systems: Electronic Structure Approaches for Biotechnology and Nanotechnology. University of Cambridge, Cambridge
16. Albert DR (2020) Monte Carlo uncertainty propagation with the NIST uncertainty machine. ACS Publications. J Chem Educ 97:1491−1494. doi:10.1021/acs.jchemed.0c00096
17. Towler M (2006) The quantum Monte Carlo method. Physica Status Solidi (b). 243(11):2573-2598. doi:10.1002/pssb.200642125
18. Cuesta S, Harikumar A, Monroy E (2022) Electron beam pumped light emitting devices. Journal of Physics D: Applied Physics 55(27):273003. doi:10.1088/1361-6463/ac6237
19. Newbury DE, Yakowitz H (1976) Studies of the Distribution of Signals in the SEM/EPMA by Monte Carlo Electron Trajectory Calculations an Outline. Use of Monte Carlo Calculations in Electron Probe Microanalysis and Scanning Electron Microscopy: Proceedings of a Workshop Held at the National Bureau of Standards, Gaithersbury, Maryland, 1-3 October 1975. Dec 1976: US Department of Commerce, National Bureau of Standards, 15.
20. Drouin D, Couture AR, Joly D et al (2007) CASINO V2. 42—a fast and easy-to-use modeling tool for scanning electron microscopy and microanalysis users. Scanning: The Journal of Scanning Microscopies 29(3):92-101. doi: 10.1002/sca.20000

21. Mintis DG, Alexiou TS, Mavrantzas VG (2020) Effect of pH and molecular length on the structure and dynamics of linear and short-chain branched poly (ethylene imine) in dilute solution: Scaling laws from detailed molecular dynamics simulations. The Journal of Physical Chemistry B. 124(28):6154-6169. doi:10.1021/acs.jpcb.0c04135

22. Mary AS, Raghavan VS, Kagula S et al (2021) Enhanced In Vitro Wound Healing Using PVA/B-PEI Nanofiber Mats: A Promising Wound Therapeutic Agent against ESKAPE and Opportunistic Pathogens. ACS Appl Bio Mater. 4(12):8466-8476. doi:10.1021/acsabm.1c00985

23. Cabal M-P, Long TE, Turos E et al (2020) Spiropiperidyl rifabutins: expanded in vitro testing against ESKAPE pathogens and select bacterial biofilms. The Journal of Antibiotics. 73(12):868-872. doi:10.1038/s41429-020-0346-x

24. Goeppert A, Czaun M, May RB et al (2011) Carbon dioxide capture from the air using a polyamine based regenerable solid adsorbent. Journal of the American Chemical Society. 133(50):20164-20167. doi:10.1021/ja2100005

25. Lin J, Lu W, Shi X et al (2021) Design of an Intelligent Nanofiber-Based Solid Amine Adsorbent with High CO2 Capture Capacity and an Ultralow Regeneration Temperature. ACS Sustainable Chemistry & Engineering. 9(30):10184-10195. doi:10.1021/acssuschemeng.1c02387

26. Mulani MS, Kamble EE, Kumkar SN et al (2019) Emerging strategies to combat ESKAPE pathogens in the era of antimicrobial resistance: a review. Frontiers in microbiology 10:539. doi:10.3389/fmicb.2019.00539

27. Santajit S, Indrawattana N (2016) Mechanisms of antimicrobial resistance in ESKAPE pathogens. BioMed Research International 2016. doi:10.1155/2016/2475067

28. Lannutti J, Reneker D, Ma T, et al (2007) Electrospinning for tissue engineering scaffolds. Materials Science and Engineering, 27(3), 504-509. doi:10.1016/j.msec.2006.05.019

29. Thomas S, Seufert B, Serrano-Garcia W et al (2022) Eco-friendly, Biodegradable, and Biocompatible Electrospun Nanofiber Membranes and Applications. In: Pathak YV, Parayil G, PatelJK (eds) Sustainable Nanotechnology: Strategies, Products, and Applications 11:173-199. doi:10.1002/9781119650294.ch11

30. Baatsen P, Gabarre S, Vints K et al (2021) Preservation of fluorescence signal and imaging optimization for integrated light and electron microscopy. Frontiers in Cell and Developmental Biology 9:737621. doi: 10.3389/fcell.2021.737621

31. Drouin D, Hovington P and Gauvin R (1997) CASINO: A new monte carlo code in C language for electron beam interactions-part II: Tabulated values of the mott cross section. Scanning 19(1):20-28. Université Sherbrooke, Québec, Canada

32. Hovington P, Drouin D, Gauvin R (1997) CASINO: A new Monte Carlo code in C language for electron beam interaction-Part I: Description of the program. Scanning 19(1):1-14. Université Sherbrooke, Québec, Canada

33. Hovington P, Drouin D, Gauvin R, et al (1997) CASINO: A new Monte Carlo code in C language for electron beam interactions-part III: stopping power at low energies Scanning, 19(1):29-35. Université Sherbrooke, Québec, Canada

34. Kyser DF (1982) Monte Carlo calculations for electron microscopy, microanalysis, and microlithography. Scanning Electron Microscopy 1982(1):10. Available at: https://digitalcommons.usu.edu/electron/vol1982/iss1/10

35. Joy D, Luo S (1989) An empirical stopping power relationship for low-energy electrons. Scanning 11(4):176-180. doi:10.1002/sca.4950110404

36. Mussakhanov D, Kobey A, Golkovski M et al (2024) Dependence of the distribution of absorbed electron flux energy in matter on the beam cross section Bulletin of the Karaganda University "Physics Series", 11629(4):168-174. doi:10.31489/2024PH4/168-174